Research Article | Vol. 7, No. 6 | 1 Jun 2017 | OPTICAL MATERIALS EXPRESS 1942
Optical Materials EXPRESS

Optical-lattice-like waveguide structures in Ti:Sapphire by femtosecond laser inscription for beam splitting

YINGYING REN,[1,2,5] LIMU ZHANG,[1] JINMAN LV,[3] YUEFENG ZHAO,[1] CAROLINA ROMERO,[4] JAVIER R. VÁZQUEZ DE ALDANA,[4] AND FENG CHEN[3,6]

[1]*Shandong Provincial Key Laboratory of Optics and Photonic Device, School of Physics and Electronics, Shandong Normal University, Jinan 250014, China*
[2]*Institute of Data Science and Technology, Shandong Normal University, Jinan 250014, China*
[3]*School of Physics, State Key Laboratory of Crystal Materials, Shandong University, Jinan 250100, China*
[4]*Grupo de Investigación en Aplicaciones del Láser y Fotónica, University of Salamanca, E-37008 Salamanca, Spain*
[5]*ryywly@sdnu.edu.cn*
[6]*drfchen@sdu.edu.cn*

Abstract: In this work, we report on the fabrication of deeply embedded optical-lattice-like structures in a Ti:Sapphire crystal by applying femtosecond laser inscription (FLI) to implement two-dimensional (2D) one-to-two and three-dimensional (3D) one-to-four beam splitting. Such a family of photonic microstructures is characterized at near-infrared both experimentally and numerically, showing excellent capability of simultaneous light confinement and beam tailoring at two orthogonal polarizations. The confocal micro-Raman image of the obtained structure reveals that the optical properties of the substrate have been well-preserved in the waveguide's active volumes. Our results pave a way to construct complex integrated waveguide splitters in Ti:Sapphire crystals by using FLI for photonic applications.

OCIS codes: (140.3390) Laser materials processing; (230.7380) Waveguides, channeled; (230.1360) Beam splitters.

References and links

1. E. Saglamyurek, N. Sinclair, J. Jin, J. A. Slater, D. Oblak, F. Bussières, M. George, R. Ricken, W. Sohler, and W. Tittel, "Broadband waveguide quantum memory for entangled photons," Nature **469**(7331), 512–515 (2011).
2. J. C. F. Matthews, A. Politi, A. Stefanov, and J. L. O'Brien, "Manipulation of multiphoton entanglement in waveguide quantum circuits," Nat. Photonics **3**(6), 346–350 (2009).
3. M. Deubel, G. von Freymann, M. Wegener, S. Pereira, K. Busch, and C. M. Soukoulis, "Direct laser writing of three-dimensional photonic-crystal templates for telecommunications," Nat. Mater. **3**(7), 444–447 (2004).
4. D. Choudhury, W. T. Ramsay, R. Kiss, N. A. Willoughby, L. Paterson, and A. K. Kar, "A 3D mammalian cell separator biochip," Lab Chip **12**(5), 948–953 (2012).
5. R. R. Thomson, R. J. Harris, T. A. Birks, G. Brown, J. Allington-Smith, and J. Bland-Hawthorn, "Ultrafast laser inscription of a 121-waveguide fan-out for astrophotonics," Opt. Lett. **37**(12), 2331–2333 (2012).
6. K. Sugioka, J. Xu, D. Wu, Y. Hanada, Z. Wang, Y. Cheng, and K. Midorikawa, "Femtosecond laser 3D micromachining: a powerful tool for the fabrication of microfluidic, optofluidic, and electrofluidic devices based on glass," Lab Chip **14**(18), 3447–3458 (2014).
7. S. Nolte, M. Will, J. Burghoff, and A. Tuennermann, "Femtosecond waveguide writing: a new avenue to three-dimensional integrated optics," Appl. Phys., A Mater. Sci. Process. **77**(1), 109–111 (2003).
8. F. Chen and J. R. V. de Aldana, "Optical waveguides in crystalline dielectric materials produced by femtosecond laser micromachining," Laser Photonics Rev. **8**(2), 251–275 (2014).
9. D. Choudhury, J. R. Macdonald, and A. K. Kar, "Femtosecond laser inscription:perspectives on future integrated applications," Laser Photonics Rev. **8**(6), 827–846 (2014).
10. K. Sugioka and Y. Cheng, "Ultrafast lasers-reliable tools for advanced materials processing," Light Sci. Appl. **3**(4), e149 (2014).
11. D. Z. Tan, K. N. Sharafudeen, Y. Z. Yue, and J. R. Qiu, "Femtosecond laser induced phenomena in transparent solid materials: Fundamentals and applications," Prog. Mater. Sci. **76**, 154–228 (2016).
12. R. Osellame, H. J. W. M. Hoekstra, G. Cerullo, and M. Pollnau, "Femtosecond laser microstructuring: an enabling tool for optofluidic lab-on-chips," Laser Photonics Rev. **5**(3), 442–463 (2011).

#291169 https://doi.org/10.1364/OME.7.001942
Journal © 2017 Received 21 Mar 2017; revised 8 May 2017; accepted 9 May 2017; published 17 May 2017

Optical Materials EXPRESS

13. R. R. Thomson, T. A. Birks, S. G. Leon-Saval, A. K. Kar, and J. Bland-Hawthorn, "Ultrafast laser inscription of an integrated photonic lantern," Opt. Express **19**(6), 5698–5705 (2011).
14. J. Burghoff, S. Nolte, and A. Tünnermann, "Origins of waveguiding in femtosecond laser-structured $LiNbO_3$," Appl. Phys., A Mater. Sci. Process. **89**(1), 127–132 (2007).
15. T. Calmano and S. Mueller, "Crystalline waveguide lasers in the visible and near-infrared spectral range," IEEE J. Sel. Top. Quantum Electron. **21**(1), 401 (2015).
16. C. Grivas, C. Corbari, G. Brambilla, and P. G. Lagoudakis, "Tunable, continuous-wave Ti:sapphire channel waveguide lasers written by femtosecond and picosecond laser pulses," Opt. Lett. **37**(22), 4630–4632 (2012).
17. Y. Ren, N. Dong, J. Macdonald, F. Chen, H. Zhang, and A. K. Kar, "Continuous wave channel waveguide lasers in Nd:$LuVO_4$ fabricated by direct femtosecond laser writing," Opt. Express **20**(3), 1969–1974 (2012).
18. A. Ródenas, G. A. Torchia, G. Lifante, E. Cantelar, J. Lamela, F. Jaque, L. Roso, and D. Jaque, "Refractive index change mechanisms in femtosecond laser written ceramic Nd:YAG waveguides: micro-spectroscopy experiments and beam propagation calculations," Appl. Phys. B **95**(1), 85–96 (2009).
19. J. Siebenmorgen, K. Petermann, G. Huber, K. Rademaker, S. Nolte, and A. Tünnermann, "Femtosecond laser written stress-induced Nd:$Y_3Al_5O_{12}$ (Nd:YAG) channel waveguide laser," Appl. Phys. B **97**(2), 251–255 (2009).
20. T. Calmano, C. Kränkel, and G. Huber, "Laser oscillation in Yb:YAG waveguide beam-splitters with variable splitting ratio," Opt. Lett. **40**(8), 1753–1756 (2015).
21. Y. Jia, C. Cheng, J. R. Vázquez de Aldana, G. R. Castillo, B. R. Rabes, Y. Tan, D. Jaque, and F. Chen, "Monolithic crystalline cladding microstructures for efficient light guiding and beam manipulation in passive and active regimes," Sci. Rep. **4**(1), 5988 (2015).
22. Y. C. Jia, C. Cheng, J. R. Vázquez de Aldana, and F. Chen, "Three-dimensional waveguide splitters inscribed in Nd:YAG by femtosecond laser writing: realization and laser emission," J. Lightwave Technol. **34**(4), 1328–1332 (2016).
23. W. Nie, Y. Jia, J. R. Vázquez de Aldana, and F. Chen, "Efficient second harmonic generation in 3D nonlinear optical-lattice-like cladding waveguide splitters by femtosecond laser inscription," Sci. Rep. **6**(1), 22310 (2016).
24. J. M. Lv, Y. Z. Cheng, J. R. Vázquez de Aldana, X. T. Hao, and F. Chen, "Femtosecond laser writing of optical-lattice-like cladding structures for three-dimensional waveguide beam splitters in $LiNbO_3$ crystal," J. Lightwave Technol. **34**(15), 3587–3591 (2016).
25. Y. Y. Ren, Y. Jiao, J. R. Vázquez de Aldana, and F. Chen, "Ti:Sapphire micro-structures by femtosecond laser inscription: Guiding and luminescence properties," Opt. Mater. **58**, 61–66 (2016).
26. V. Apostolopoulos, L. Laversenne, T. Colomb, C. Depeursinge, R. P. Salathe, M. Pollnau, R. Osellame, G. Cerullo, and P. Laporta, "Femtosecond-irradiation-induced refractive-index changes and channel waveguiding in bulk Ti^{3+}: Sapphire," Appl. Phys. Lett. **85**(7), 1122–1124 (2004).
27. J. Siebenmorgen, K. Petermann, G. Huber, K. Rademaker, S. Nolte, and A. Tunnermann, "Femtosecond laser written stress-induced Nd:$Y_3Al_5O_{12}$ (Nd:YAG) channel waveguide laser," Appl. Phys. B **97**(2), 251–255 (2009).
28. L. Wang, F. Chen, X. L. Wang, K. M. Wang, Y. Jiao, L. L. Wang, X. S. Li, Q. M. Lu, H. J. Ma, and R. Nie, "Low-loss planar and stripe waveguides in Nd^{3+}-doped silicate glass produced by oxygen-ion implantation," J. Appl. Phys. **101**(5), 053112 (2007).

1. Introduction

Over the past decade, integrated photoniccircuits based on optical waveguide structures have experienced a significant progress, making them by no means a laboratory curiosity but potential miniature devices that demonstrate widespread applications in fields such as telecommunication, bio-photonic and optical astronomy [1–5]. This can be largely attributed to the rapid development of modern micromachining technologies for the fabrication of optical waveguides. Femtosecond laser inscription (FLI), as an example of these technologies, has shown its unprecedented capabilities for 3D waveguiding device fabrication [3–10]. By locally modifying the refractive index (RI) of the material through nonlinear absorption of the incident radiation [11], optical waveguide structures can be produced within the bounds of the substrate. The most intriguing advantage of FLI is its flexibility not only in term of the design freedom of waveguide geometry but also in the broad material applicability. Benefiting from this, 3D splitters based on waveguide structures have been produced in plenty of optical materials. Glass based materials are considered as one of the most appropriate substrates for splitter formation by utilizing FLI with single- or multi-scan techniques, in which a localized increase of RI is usually induced in contrast to the unirradiated bulk, constructing splitting devices based on so called Type-I waveguides [5,7,12,13]. R. R. Thomson *et al.* demonstrated a 121-waveguide fan-out device [5] and a 3D integrated photonic lantern [13] in borosilicate glass for astro-photonic application, which manifest the ability of FLI as a real 3D direct writing technique and underscore its aforementioned advantages. Nonetheless, in the overwhelming majority of crystalline media, negative RI changes are typically induced within

Optical Materials EXPRESS

the laser damage regions [8,14]. In this case, Type-II structure that consists of two damaged tracks surrounding an unirradiated area is required, which can regulate the beam propagation through the strain-optic effect [15–21]. Unfortunately, the benefit of simplification in the manufacturing of Type-II-structure-based splitters is often mitigated by its infeasibility for three-dimensional beam splitting as well as its poor confinement of light under certain polarization. An alternative solution is the implementation of a new class of monolithic instruments based on the optical-lattice-like (OLL) structures, which was firstly demonstrated by Jia *et al.* in 2014 [21]. Such a structure contains several evenly distributed tracks inscribed by FLI with missing tracks acting as lattice defects. Due to the RI contrast between laser-induced low-index tracks and intact cores (i.e. lattice defects), efficient light confinement and mode conversion are allowed along the arrangement of lattice defects. The insightful merits of OLL-structures lie in their designability and flexibility. The creation of such structures exploits a method to construct compact and robust geometry for any demanded splitting manners in 3D form. Up till now, OLL-structure-based splitters have been produced in Nd:YAG [21,22], KTP [23] and $LiNbO_3$ [24] crystal wafers for one-to-two, one-to-three or one-to-four beam splitting, realizing, in active regime, near-infrared laser excitation [21,22] and second harmonic generation of green light [23]. Furthermore, the laser guidance of OLL-splitters in Nd:YAG and KTP are found to be polarization-independent, showing excellent isotropic light confinement capabilities.

Ti:Sapphire, as a well-established material, is attractive for its large gain bandwidth. Waveguide structures based on Ti:Sapphire crystals have been demonstrated for wide spectral luminescence generation and tunable laser ranging from ~600 nm to ~1000 nm [16,25,26]. In this work, we demonstrate, for the first time to our knowledge, the fabrication and characterization of highly-compact and deeply-embedded beam splitters in Ti:Sapphire crystal by using FLI based on hexagonal/dual-hexagonal OLL-architectures. In addition, a straightforward hexagonal OLL-waveguide is produced for comparison. The performances of these structures as passive devices regarding the guiding and splitting properties at near-infrared wavelength are investigated experimentally and numerically.

2. Experiments in details

The splitting devices are fabricated in a Ti:Sapphire crystal wafer (0.15 wt% Ti_2O_3), which is cut into a dimension of 10(a) × 2(b) × 5(c) mm^3 and then optically polished. Structures are inscribed using a Ti:Sapphire laser system (Spitfire, Spectra Physics, USA) with the laser facility of the Universidad de Salamanca as previously reported in [25]. The system delivers 120 fs pulses of 795 nm radiation at a pulse repetition frequency of 1 kHz. The Ti:Sapphire crystal wafer is mounted on an XYZ stage, which facilitates a precise translation of the sample through the laser focus at a speed of 500 μm/s in the direction parallel to the 10-mm edge (a-axis). The linearly-polarized laser beam is focused into the sample using a microscope objective with a numerical aperture of 0.4. The laser polarization is perpendicular to sample translation direction. All structures formed in this work are inscribed using 1.2-μJ pulse energy. Under these conditions, the laser inscribed tracks are found to have a cross-sectional length of 10 μm along b-axis of the Ti:Sapphire substrate.

By applying FLI technology in Ti:Sapphire with the aforementioned parameters, hexagonal and dual-hexagonal OLL-structure based splitters are produced, both of which consist of three parts of equal length (~3.3 mm) connected in sequence, as shown in Fig. 1(a) and Fig. 2(a). For the structural fabrication, the separation between two adjacent tracks is set to be 10 μm and the maximum focusing depth is around 250 μm beneath the crystal surface. Figure 1(b) shows separately the schematics of the three parts of the OLL-splitter designed for one-to-two beam splitting (hereafter OLL-Sp1). It can be found that the transverse separation between the centers of two output channels in Part III is 30 μm. Similarly, one-to-four beam transformation is implemented based on the combination of 3 parts of dual-hexagonal OLL-structures (OLL-Sp2), as shown in Fig. 2(b). The separation distances

Optical Materials EXPRESS

between the output core centers along b- and c-axes are 60 μm and 30 μm, respectively. According to the design concept, along with the expansion of core region in Part II of each structure, an additional damaged track is introduced to the central axis of the structure. Consequently, single mode from the input waveguide (i.e. Part I) could be manipulated to double mode with each mode located near the branch region of output waveguide (i.e. Part III). Hence, Part II can be considered as a transition between Part I and Part III. The splitting ratios between the branched arms are designed to be 1 for both OLL-splitters. Additionally, for comparison, a straightforward OLL-waveguiding structure (OLL-Wg) is manufactured in the sample along a-axis with a length of 10 mm and the same morphology as the Part I of OLL-Sp1. Such a straight OLL-structure is used as a reference.

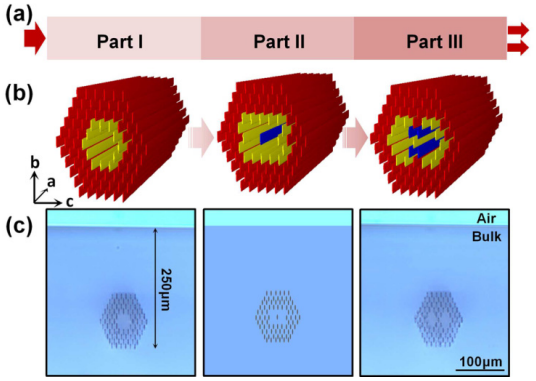

Fig. 1. (a) The prototype of the OLL-structure based beam splitter with connection of Part I, II and III. The schematic images (b) and the cross-sections (c) of Part I-III of hexagonal OLL-splitter designed for one-to-two beam splitting (OLL-Sp1). For clarity, the laser-induced tracks in (b) are displayed with different colors. Please note that the middle figure of (c) is plotted according to the design concept rather than observed with optical microscope.

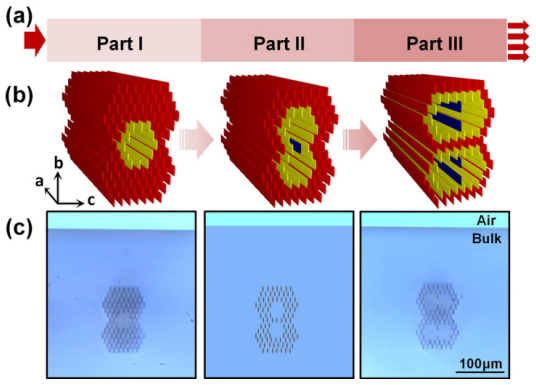

Fig. 2. (a) The prototype of the OLL-structure based beam splitter with connection of Part I, II and III. The schematic images (b) and the cross-sections (c) of Part I-III of dual-hexagonal OLL-splitter designed for one-to-four beam splitting (OLL-Sp2). For clarity, the laser-induced tracks in (b) are displayed with different colors. The middle figure of (c) is plotted according to the design concept.

The abilities of resulting structures at near-infrared wavelength (1064 nm) are experimentally characterized with typical end-face coupling arrangements. The modal profiles of the guided modes at two orthogonal polarizations are investigated. Based on the numerical array data of modal profiles, the laser intensity generated from each output port can be calculated, and afterwards the intensity splitting ratios could be determined. In addition, the 1064-nm light propagations in the formed splitters are simulated by the commercial program BeamPROP (Rsoft, Inc). For this purpose, RI contrast of OLL-Wg is estimated

Optical Materials EXPRESS

roughly by measuring its maximum incident angle based on the method introduced by Siebenmorgen *et al.* [27]. To investigate the polarization-dependence of the splitters, a halfwave plate is employed to continuously vary the polarization of a linearly polarized incident laser. The total attenuations of the waveguide splitters including splitting losses and propagation losses at 1064 nm are determined by directly detecting the incident and output beam power while considering the Fresnel reflection losses at both end-facets, the coupling efficiency and the transmittance of microscope objective lens, as previously introduced in Ref [28]. Furthermore, in order to assess the waveguide quality and, in parallel, explore preliminarily the mechanism behind the waveguide formation from the perspective of Raman scattering, further investigation on micro-Raman (μ-Raman) confocal mapping analysis of the guiding structures is performed by utilizing the Renishaw inVia Reflex Raman microscope.

3. Results and discussion

The optical microscopic images of the input and output facets of splitters OLL-Sp1 and -Sp2 are shown in Fig. 1(c) and Fig. 2(c), respectively. Please note that, for easy visualization and comparison, the end views of Part II which are not in the position to be detected directly with optical microscope are plotted according to the design concept of two splitters, as seen from the middle figures of Fig. 1(c) and Fig. 2(c). As can be clearly observed, the materials in the region of tracks are appropriately modified, without inducing any damage in the core regions. Moreover, these structures are produced deeply embedded in the substrate without modifying the materials on the surface. Hence, more superficial structures could be introduced on the sample surface, meeting the requirement of circuit integration for compact lab-on-a-chip photonic devices.

As a representative, the output facet of OLL-Sp1, as shown in Fig. 3(a), is used for a continuous μ-Raman intensity mapping within a wide area covering the modified and unmodified volumes. The experimental result is displayed in Fig. 3(b) in 2D plot. In this mapping figure, the damage tracks are revealed by the intensity quenching of spectral lines. The Raman reduction in the laser-damaged tracks in a first order approximation can be attributed to the creation of high density of lattice defects and imperfections, which is responsible for the RI decrease in these areas and hence related to the formation of waveguiding structures [18]. Furthermore, in two output channels of OLL-Sp1, the Raman intensity is not deteriorated during the FLI procedure in respect to bulk, suggesting that the excellent properties of Ti:Sapphire substrate are expected to be fairly well preserved in guiding areas and therefore showing the potential of active applications of these structures for luminescence or laser emissions.

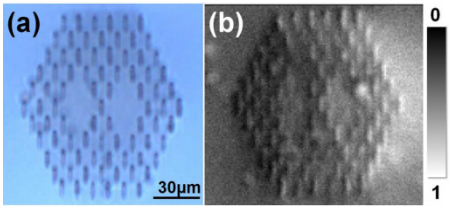

Fig. 3. (a) The microscopic view of the output facet of OLL-Sp1 with two distinct waveguide channels. (b) The μ-Raman intensity mapping result of the waveguide cross-section.

Parallel studies are performed to characterize and compare the properties of OLL-structure based splitters and straight OLL-waveguide. Figures 4(a) and 4(b) display the measured near-field intensity (normalized) distributions of OLL-Wg for TE and TM polarizations at 1064 nm, showing the Gaussian-type profiles. This waveguide is found to be single-mode at TM polarization and capable of guiding high-order TE modes at near-infrared wavelength, as evidenced by the insert figures in Fig. 4(a) for TE_{01} and TE_{10} modes. However, the high-order mode guidance is difficult to excite and under this condition the coupling efficiency is not as

Optical Materials EXPRESS

high as that of single-mode guidance. Therefore, the characterizations of these splitters are investigated with the best coupling condition under which fundamental mode or single mode is excited in Part I of each waveguide. Figures 4(c) and 4(d) depict the measured TE and TM laser modes of one-to-two splitter at wavelength of 1064 nm. The two distinct modes under either polarization suggest the impressive ability for beam tailoring of OLL-Sp1. More attractively, owing to the contraction of waveguide volumes, single-mode guidance are obtained from the output channels of OLL-Sp1 at either polarization, which is an intriguing feature of this device for its application on photonic circuits. By calculating the output power from each arm of the OLL-Sp1, the one-to-two beam splitting ratio is determined to be around 0.96 (left arm): 1 (right arm) for TM transmission mode, which indicates an equalization of the incident beams. Similarly, Figs. 4(e) and 4(f) illustrate the experimental near-field intensity distributions from the output of the one-to-four beam splitter (OLL-Sp2) for TE and TM modes at 1064 nm, indicating the realization of real 3D beam splitting along both lateral and longitudinal orientations. The intensity splitting ratio of OLL-Sp2 under TM polarization is calculated to be 0.98:0.95:1:0.89 for four arms (top left: top right: bottom left: bottom right).

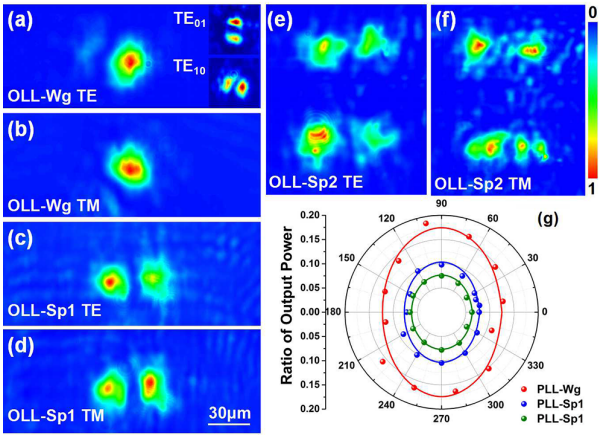

Fig. 4. (a)-(f) The measured TE and TM mode distributions of OLL-structures at 1064 nm. The insets of (a) show TE_{01} and TE_{10} modes of straight forward waveguide OLL-Wg. (g) Polarization dependency of OLL-structures. The red, blue and green balls represent the experimental results for OLL-Wg, OLL-Sp1 and OLL-Sp2, respectively. The solid lines are elliptical fit of experiment data.

To further investigate the polarization-dependence of OLL-structures, the 1064-nm laser transmissions along the transverse plane through these structures are measured while rotating the halfwave plate and therefore all-angle powers are achieved, as shown in Fig. 4(g), in which 0°/180° correspond to TE polarization and 90°/270° relate to TM polarization. The resultant elliptical curves suggest slight polarization sensitivity of these structures, which is mainly due to the anisotropy of Ti:Sapphire crystal along b- and c- axes. Nevertheless, the guidance exists for any transverse polarizations for all structures, which suggests good symmetry and smoothness of the fabricated structures, making them ideal platforms for unpolarized pumping as light sources. Based on the ratios of output power to the input power shown in Fig. 4(g), the total attenuations of OLL-Sp1 along TE and TM polarization are calculated to be 6.4 dB and 5.3 dB, respectively. By comparing these experimental values with the propagation losses of hexagonal straight waveguide (*i.e.* OLL-Wg) which are 4.5 dB (TE) and 2.9 dB (TM), the splitting losses of the splitter OLL-Sp1 can be determined to be 1.9 dB and 2.4 dB for TE and TM modes. The total losses of one-to-four beam splitter (OLL-Sp2) further increase to 7.2 dB and 6.4 dB for TE and TM polarizations because of the increment of additional splitting losses. One can expect the reduction of losses by optimizing

Optical Materials EXPRESS

the inscription parameters and post-processing treatment (such as through thermal annealing treatment). Furthermore, taking advantage of the flexibility of OLL-splitters, more transitional structures could be fabricated and inserted between input and output sections, making the mode transforming more slowly and smoothly along the waveguide and hence reducing the splitting losses effectively.

The beam profile evolution of 1064-nm light propagating along OLL-splitters under TM polarization is simulated based on the reconstructed spatial distribution of RI which is estimated preliminarily to be 4.8×10^{-3}. In order to determine the accurate value of RI, the output mode profile of each splitter is simulated with different RI, ranging from 3.0×10^{-3} to 7.0×10^{-3} in a step of 0.1×10^{-3}. By comparing the simulated results with the measured mode distributions in Fig. 4, the RI contrast of formed structure is ultimately determined to be 6.0×10^{-3}. Under this situation, the best agreement between the simulated and experimental results is achieved, as shown in Fig. 5. It is worth to point out that this value of RI contrast applies to all structures fabricated in this work due to the identical writing conditions. It could be found that, the simulated beam evolution processes are in accordance with the design philosophy for one-to-two and one-to-four beam splitting. In addition, as one can see, the modal profiles of waveguide beam splitters at the output ends based on the simulations are in reasonable agreement with the results experimentally achieved (Figs. 4(d) and 4(f)).

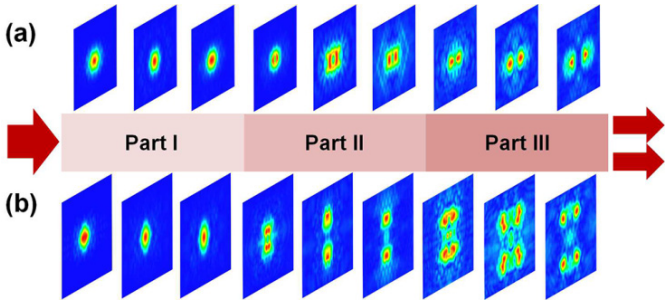

Fig. 5. Simulated modal profile evolution of one-to-two (a) and one-to-four (b) OLL-splitters at 1064 nm.

4. Summary

In summary, we demonstrate the design and fabrication of monolithic waveguide beam splitters in a Ti:Sapphire crystal. By employing the powerful FLI technology, the deeply-embedded one-to-two and one-to-four splitters are produced based on hexagonal/dual-hexagonal OLL-architectures without any deterioration in the optical properties of substrate in the guiding cores. The fabricated splitters exhibit capability of supporting orthogonal polarizations under near-infrared with acceptable splitting ratios. More attractively, single-mode guidance is achieved from one-to-two beam splitter. The good performances of these structures make them extremely promising for constructing miniature devices and integrated optical circuits for various applications in both passive (*e.g.* mode convertor and beam splitter) and active (*e.g.* generation of broadband luminescence and tunable laser) regimes.

Funding

National Natural Science Foundation of China (No.11404194 and No. 11404196); Junta de Castilla y León (Project SA046U16); MINECO (FIS2015-71933-REDT).

Acknowledgments

This work is supported by the National Natural Science Foundation of China (No.11404194 and No. 11404196). Authors acknowledge support from Junta de Castilla y León (Project SA046U16) and MINECO (FIS2015-71933-REDT). Authors would like to thank Prof. Ajoy.

Optical Materials EXPRESS

K. Kar and Dr. Mark D. Mackenzie from Heriot-Watt University for their help on μ-Raman intensity measurement.